Facile Synthesis and Characterization of Fe/FeS Nanoparticles for Environmental Applications

ARTICLE *in* ACS APPLIED MATERIALS & INTERFACES · MAY 2011

Impact Factor: 6.72 · DOI: 10.1021/am200016v · Source: PubMed

ACS APPLIED MATERIALS & INTERFACES

RESEARCH ARTICLE

www.acsami.org

Facile Synthesis and Characterization of Fe/FeS Nanoparticles for Environmental Applications

Eun-Ju Kim,[†] Jae-Hwan Kim,[†] Abdul-Majeed Azad,[‡] and Yoon-Seok Chang*[,†]

[†]School of Environmental Science and Engineering, Pohang University of Science and Technology (POSTECH), Pohang, 790-784, Korea

[‡]Department of Chemical Engineering, The University of Toledo, Toledo, Ohio 43606-3390, United States

ABSTRACT: Multicomponent nanoparticles containing two or more different types of functionalities show unique physical and chemical properties, leading to significantly enhanced performance. In this study, we have developed a new one-pot method to prepare Fe/FeS nanoparticles using dithionite at room temperature. The FeS precipitates on the Fe surface are formed by the interaction between dissolved iron species and hydrogen sulfide, one of the decomposition products of dithionite in solution. The resulting Fe/FeS nanoparticles have high surface area, good electrical conductivity, and strong magnetic responsivity. In addition, the Fe/FeS shows a much higher reactivity toward contaminants than the pure Fe nanoparticles. The above synthesized nanoparticles are successfully applied for the rapid removal of trichloroethylene (TCE) from water. The study reveals that Fe/FeS nanoparticles are a promising candidate for the efficient removal of pollutants.

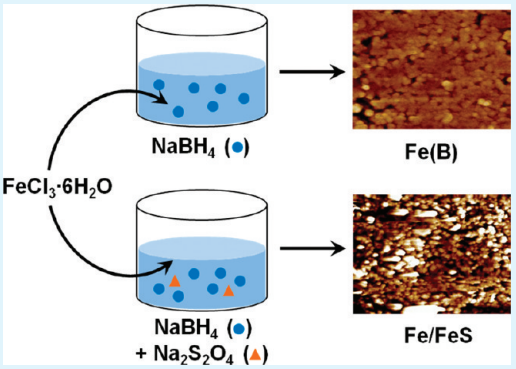

KEYWORDS: multicomponent nanoparticles, dithionite, iron sulfides, zerovalent iron, TCE

1. INTRODUCTION

Multicomponent nanoparticles have received considerable attention because they provide novel functions not available in single-component nanoparticles. The multicomponent nanoparticles can possess unique physical and chemical properties due to complementary or synergistic effects induced by interactions between the different components.[1] They have great potential for a wide range of applications including biological separation, controlled release of drugs, catalysis, and contaminant removal.[2−7] There are several ways to obtain the hybrid nanoparticles with desired structures and properties.[8−13] However, the existing procedures involve quite complicated and time-consuming steps, thus rendering the whole process too costly for practical applications. Therefore, research efforts have been expended toward developing new and simple synthetic approaches to produce multicomponent nanoparticles.

Iron sulfides refer to several types of compounds containing iron and sulfur with a formula of $Fe_{1+\chi}S$ or $Fe_{1-\chi}S$. The crystal shapes and physical properties of iron sulfides change significantly depending on the variation of iron content.[14] Recently, iron sulfides are recognized as a valuable inorganic material in many areas, especially environmental remediation because of its chalcophilic nature and reducing capability.[15−17] For example, iron sulfides exhibit a high affinity for heavy metals and chlorinated pollutants.[18−22] It is expected that the improved catalytic properties can be achieved by a combination of iron sulfides and zerovalent metals. Although several studies have addressed the effect of sulfur compounds on iron-mediated dechlorination, the exact mechanism of the process has not been elucidated yet.

In this paper, we describe a novel method for the preparation of iron/ferrous sulfide nanoparticles (Fe/FeS) using sodium dithionite ($Na_2S_2O_4$). Dithionite is a general reducing agent widely used in research and industry,[23,24] owing to the moderate cost and relatively nontoxic nature. It is quite unstable and decomposes rapidly in aqueous solutions.[25] Dithionite has been chosen because its decomposition releases hydrogen sulfide and such side reactions can readily induce the precipitation of insoluble FeS on iron surface as below:[26,27]

$$2S_2O_4^{2-} + H_2O \rightarrow 2HSO_3^- + S_2O_3^{2-} \quad (1)$$

$$S_2O_4^{2-} + S_2O_3^{2-} + 2H_2O + H^+ \rightarrow H_2S + 3HSO_3^- \quad (2)$$

$$H_2S \rightarrow 2H^+ + S^{2-} \quad (3)$$

$$Fe^{2+} + S^{2-} \rightarrow FeS \quad (4)$$

In our process, generation of Fe^0 and FeS via in situ precipitation occurs simultaneously in one-pot that offers advantages of simplicity, ease, and rapidity.

The objective of our work is to produce Fe/FeS nanoparticles via a facile chemical conversion route by simply adding dithionite. The resulting Fe/FeS had high surface area, good electrical conductivity, and strong magnetic responsivity. Moreover, Fe/FeS showed strong reactivity toward contaminants in water.

Received: January 6, 2011
Accepted: April 26, 2011
Published: April 26, 2011

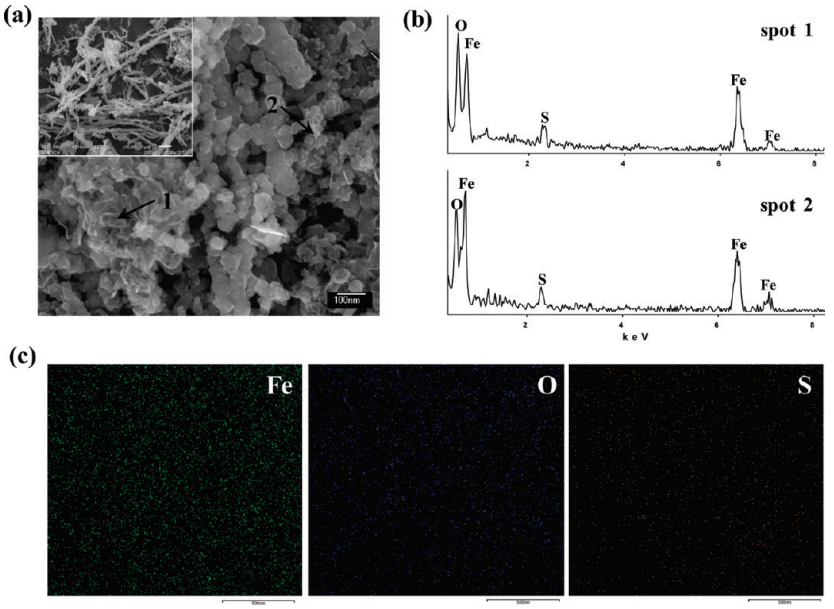

Figure 1. SEMs of Fe/FeS nanoparticles: (a) Low (inset) and high-magnification images; (b) EDX spectra recorded from two spots in a; (c) corresponding X-ray maps for Fe, O, and S.

Trichloroethylene (TCE) was chosen as a model compound since it is a most common and troublesome groundwater pollutant. The Fe/FeS was successfully applied to fast and efficient removal of TCE from water. Ease of synthesis and the potential for degrading pollutants can make these materials an ideal applicant for environmental remediation. Furthermore, to the best of our knowledge, this is the first report on the synthesis of Fe/FeS nanoparticles.

2. EXPERIMENTAL SECTION

Chemicals and Materials. Sodium dithionite ($Na_2S_2O_4$, 80+%) was obtained from Fluka. Trichloroethylene (TCE, 99+%), *cis*- and *trans*-1,2-dichloroethylene (1,2-DCE, 98+%), ferric chloride ($FeCl_3 \cdot 6H_2O$, 98+%), and sodium borohydride ($NaBH_4$, 98+%) were supplied by Sigma-Aldrich. Concentrated HCl (37%) and ethanol (ACS grade) were purchased from Merck. All the solutions used in were prepared with ultrapure water (resistivity: 18.3 MΩ cm) which was degassed with high-purity N_2 for 2 h.

Commercial reactive nanoscale iron particles (RNIP) were purchased from Toda Kogyo Corp. (Onoda, Japan). Prior to use, the particles were centrifuged and washed three times with deoxygenated water. Fe nanoparticles (Fe(B)) were prepared by reducing 0.5 M $FeCl_3$ with 0.8 M $NaBH_4$, based on Kim's method.[28] FeS was synthesized by mixing 2.0 L of 0.57 M $FeCl_2$ with 1.2 L of 1.1 M Na_2S in an anaerobic chamber for 3 days. After discarding the supernatant, the solid was washed 8 times with fresh deoxygenated water. Jeong et al.[29] reported that the particle size of FeS obtained from this method was 3.5−35 nm.

Synthesis of Fe/FeS Nanoparticles. Fe/FeS nanoparticles were synthesized using a modified borohydride reduction method with dithionite. Briefly, appropriate amounts of dithionite (0.1, 0.5, 1.0, 2.0, and 5.0 g) were dissolved in 1 L of 0.8 M $NaBH_4$ for samples referred to as Fe/FeS 1 to Fe/FeS 5, respectively. The resulting solution was then added dropwise to 0.5 M $FeCl_3$ in a 3:1 volume ratio. The remaining solution was decanted, and the precipitates were rinsed with degassed water several times. The particles were dried in a vacuum oven for 1 d and stored in an anaerobic chamber prior to characterizations.

Characterization. The surface composition and morphology were investigated by a JEOL JSM-7401F scanning electron microscopy (SEM)/energy dispersive X-ray (EDX) system at 15 kV. X-ray diffraction (XRD) analyses were carried out at room temperature with Cu Kα radiation on a MXP18 HF diffractometer (MAC Science Co., Japan). The patterns were collected between 10 and 80° (2θ) at a scan rate of 5.0° 2θ/min. The X-ray photoelectron spectroscopy (XPS) spectra were obtained by a VG ESCALAB 220iXL using monochromatic Mg Kα (1253.6 eV) excitation source. The narrow scans over the selected binding energy range of 156.6−176.6, 181.6−199.6, and 696.6−729.6 eV were used to discern the chemical state of sulfur, boron, and iron, respectively. Correction for surface charging was made with reference to C 1s peak at 285 eV. Atomic force microscopy (AFM)/electrostatic force microscopy (EFM) imaging was performed on a Digital instrument Nanoscope V (Veeco, USA). For these tests, the dried samples were pressed into pellets using a hydraulic press. The BET (Brunauer−Emmett−Teller) specific surface area was measured by N_2 adsorption method using an ASAP 2010 system (Micromeritics Corp., USA). The saturation magnetization was determined at 300 K with a magnetic property measurement system XL-7 (Quantum Design, USA) under a maximum field of 50 kOe. E_h value was measured using an Orion ORP combination electrode (Thermo Scientific, USA).

Application of Fe/FeS Nanoparticles to Removal of TCE and Analysis. TCE removal efficiency of Fe/FeS nanoparticles was compared with two types of pure Fe nanoparticles (RNIP and Fe(B)) and FeS. Batch tests were performed in 35 mL amber colored glass vials capped with Teflon Mininert valves. Aqueous TCE (15 mg/L) was added to the vials with 0.08 g of the materials. Controls including only TCE solutions were also prepared to evaluate the loss of TCE due to adsorption and volatilization under identical experimental conditions. The vials were then placed on a rolling mixer (15 rpm) at 26 ± 1 °C. All experiments were done in duplicate.

The aqueous concentrations of TCE and its chlorinated products were determined by headspace gas chromatography equipped with an electron capture detector (GC-ECD) (HP Agilent 6890, USA). A 1.0 mL portion of the aqueous phase was withdrawn periodically during the reaction and transferred into the vial (22-mL) containing 9.0 mL of water. The vials were shaken at 80 °C for 15 min, and then 1.0 mL of

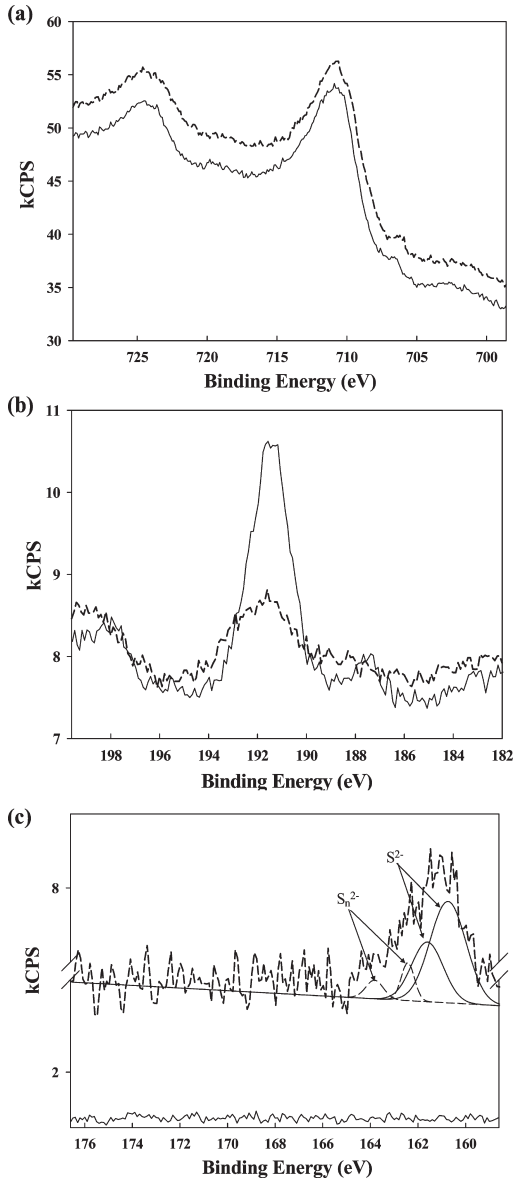

Figure 2. Narrow scans of (a) Fe(2p), (b) B(1s), and (c) S(2p) XPS spectra. The solid and dashed lines represent Fe(B) and Fe/FeS, respectively.

headspace was automatically injected into GC system. The initial oven temperature was kept at 60 °C for 1 min and increased to 180 °C at a rate of 10 °C/min.

3. RESULTS AND DISCUSSION

Characterization of Fe/FeS Nanoparticles. The XRD pattern of Fe/FeS (data not shown) showed the characteristic reflections for α-Fe^0 at 44.3 and 65.2° (2θ). A weak and broad peak at 35° was ascribed to ferric oxide. However, sulfur-bearing compounds, such as FeS or FeS_2, could not be discerned in the pattern, due mainly to their low concentration or low degree of crystallinity. Some discrepancies could also be found in the literature with regard to the XRD data of the precipitated iron sulfides.[30]

The nanoparticles were investigated by field emission scanning electrom microscopy (FE-SEM) in conjunction with EDX analysis and elemental mapping of Fe, O, and S. The freshly prepared Fe/FeS showed chain-like aggregates of spherical particles (Figure 1a). EDX spectra at two locations in Figure 1a contained peaks of S as well as Fe and O (Figure 1b); oxygen peaks could be due to the adsorbed oxygen or facile oxidation of the particles. The elemental maps (Figure 1c) clearly suggest that sulfur is uniformly distributed within the particles which is predominantly iron (80.9%, by weight). The presence of sulfur is expected to originate from dithionite used in the synthesis of this product. RNIP (Toda, Japan) also contains unidentified sulfur fraction, and the manufacturer claims that sulfur present in their sample plays an important role in the reactivity.

Table 1. Specific Surface Areas and Roughness Values of Fe/FeS and Fe(B)

materials	BET surface area (m^2/g)	AFM R_{rms} value (nm)	EFM R_{rms} value (deg)
Fe/FeS 1	25.6 (±0.3)	16.6 (±2.3)	0.34 (±0.04)
Fe/FeS 2	31.4 (±0.2)	20.1 (±3.1)	0.61 (±0.06)
Fe/FeS 3	32.9 (±0.1)	21.7 (±1.6)	0.70 (±0.02)
Fe/FeS 4	42.2 (±0.3)	30.3 (±4.1)	1.05 (±0.10)
Fe/FeS 5	35.1 (±0.2)	34.1 (±2.9)	1.21 (±0.12)
Fe(B)	24.9 (±0.1)	13.2 (±1.1)	0.21 (±0.03)

XPS measurements were carried out to determine the chemical state of sulfur on the Fe/FeS. Figure 2 compares the XPS spectra of Fe(B) and Fe/FeS in the Fe (2p), B (1s) and S (2p) regions. The elemental composition was calculated by using peak areas and appropriate sensitivity factors. In the case of Fe(B), the surface composition was mainly iron and boron (43.9 and 56.1 at.%, respectively), while Fe/FeS showed the presence of sulfur as well (Fe: 57.2, B: 36.8, and S: 6.0 at %, respectively). Fe (2p) spectra give weak Fe(0) and strong Fe(III)-O peaks for both materials (Figure 2a). Considering that a sampling depth of XPS is less than 5 nm, the Fe spectra indicate the core/shell structure, consistent with an iron core coated with a thin layer of iron oxide. Exposure of Fe nanoparticles to air seemed to contribute to the low Fe(0) content during the template preparation and setting. In the Fe (2p) region of Fe/FeS, FeS compounds near 707.1 ± 0.1 eV were not detected, perhaps because of their low levels and partial oxidation. Indeed, FeS is very reactive toward oxygen, which easily transforms to greigite (Fe_3S_4) and iron oxide.[30] The B (1s) peaks at 187.6 and 191.5 eV in Fe(B) could be assigned to reduced boron (as boride) and oxidized boron (as borate), respectively (Figure 2b). However, Fe/FeS exhibited a single borate peak and its intensity decreased considerably compared to that in Fe(B). In the S (2p) spectrum of Fe/FeS, a broad single peak was fitted with two doublets at 161.2 ± 0.2 and 163.4 ± 0.4 eV (Figure 2c). These typically corresponded to sulfide (S^{2-}) and polysulfide (S_n^{2-}) species. The polysulfide species reveal that some oxidation of the surface may have occurred.[31] Therefore, the combined results of SEM/EDX and XPS analysis support the presence of low density FeS on the Fe surface.

The effect of dithionite concentration on surface structure was further characterized by AFM/EFM analysis and surface area measurements. The results were summarized in Table 1. AFM/EFM was performed to evaluate the changes in surface topography and electronic properties caused by the presence of FeS. The surface heterogeneity was determined by measuring the root-mean-square roughness (R_{rms}) value within a given area.[32]

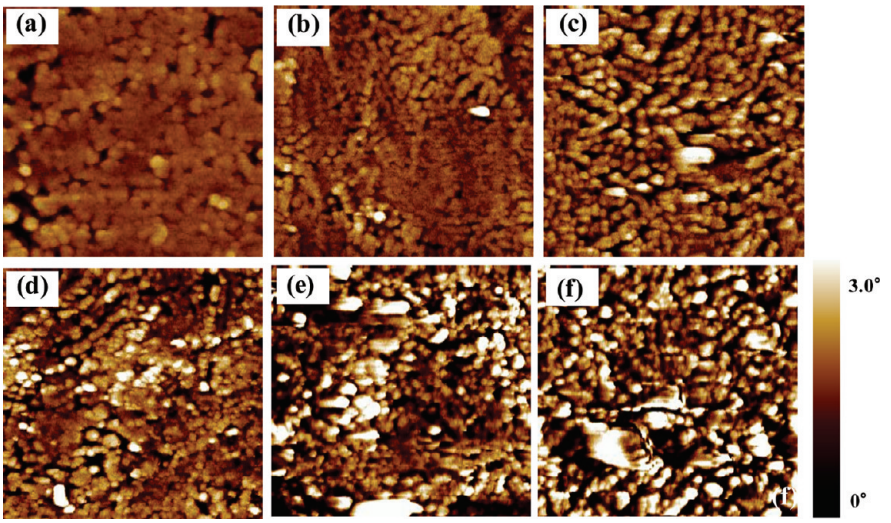

Figure 3. EFM images of (a) Fe(B), (b) Fe/FeS 1, (c) Fe/FeS 2, (d) Fe/FeS 3, (e) Fe/FeS 4, and (f) Fe/FeS 5.

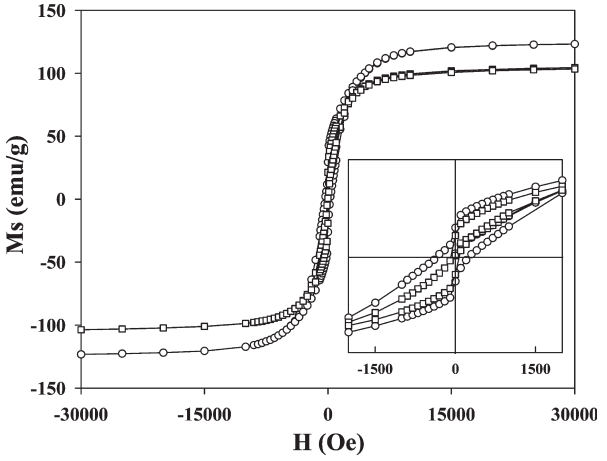

Figure 4. Magnetization curves at room temperature for Fe(B) (circles) and Fe/FeS (squares): (inset) results in low-field region.

Fe(B) had a relatively smooth and uniform surface compared to Fe/FeS. When dithionite concentration increased from 0.1 to 5.0 g/L, the R_{rms} values gradually increased (Table 1). A significant increase in surface roughness of the nanoparticles could be due to the formation of FeS precipitates. Several researches have suggested that surface modification of iron such as pit formation and roughness change can cause dramatic improvement in the removal efficiency.[33,34] For example, the coarse and rough surfaces with higher fraction of edge areas has a higher reaction rates than the smooth surfaces. In the case of Fe/FeS, the rate of the overall process can be increased through the contaminant accumulation on the rough surface. In addition, Park et al.[35] propose that the FeS mineral in aqueous solution tends to be less hydrated than iron oxide and carry more hydrophobic sites; the hydrophobic TCE is likely to be more easily attracted to FeS surface for subsequent electron transfer processes.

The EFM images in Figure 3 were taken by applying a bias of +5 V to the tip. EFM is a useful technique to characterize the surface potential and conductivity change. The differences between the conducting and nonconducting surfaces can be determined by the phase brightness and roughness values (R_{rms}); the phase roughness is indicative of electrostatic field gradient. The R_{rms} value increased with increasing dithionite concentration, which was consistent with the results obtained from AFM analysis (Table 1). Fe/FeS 5 showed much better brightness and almost a 6 times higher R_{rms} value (1.21°) than that of Fe(B) (0.21°). This suggests that the electron flow on the Fe/FeS surface exhibited good mobility. Iron sulfides are generally known as either semiconductors or metallic conductors due to the presence of delocalized electrons in the layers. Consequently, the deposition of FeS on the iron surface can facilitate conduction of electrons from iron core to adsorbed TCE, thereby resulting in the remarkable rate enhancement of TCE reduction.

The multipoint BET method was used to calculate the specific surface area of Fe/FeS. Here, the surface area of Fe/FeS 4 was determined as 42.2 ± 0.3 m^2/g, which was greater than that previously reported for pure Fe (21−33 m^2/g).[36,37] The surface area of the nanoparticles was found to increase linearly as dithionite concentration increased from 0.1 to 2.0 g/L. However, with further dithionite addition, the surface area decreased, which is likely due to pore plugging and masking by excessive FeS precipitates.

Magnetic Properties of Fe/FeS. Figure 4 displays the hysteresis loops of the pure Fe and Fe/FeS at room temperature, revealing a ferromagnetic behavior. These samples exhibited typically soft magnetic features such as low coercivity and high permeability.[38] In fact, iron-based particles have long been used as soft magnetic materials. Both Fe and Fe/FeS reached magnetic saturation in relatively low applied fields. The saturation magnetization (Ms, 103.1 emu/g) of Fe/FeS was slightly lower than that of the pure Fe (120 emu/g). The reduced coercivity and Ms value of the synthesized Fe/FeS compared with pure Fe may be attributed to the exchange coupling between the FeS and Fe phases.

Potential Application of Fe/FeS Nanoparticles for Removing TCE. The feasibility of Fe/FeS for the removal of pollutants from aqueous solutions was examined using TCE as a model compound. Figure 5a shows the reduction kinetics of TCE by Fe/FeS synthesized under varying dithionite concentrations. The degradation profiles were well fitted to a pseudo-first-order model. As presented in Figure 5b, the observed first-order rate

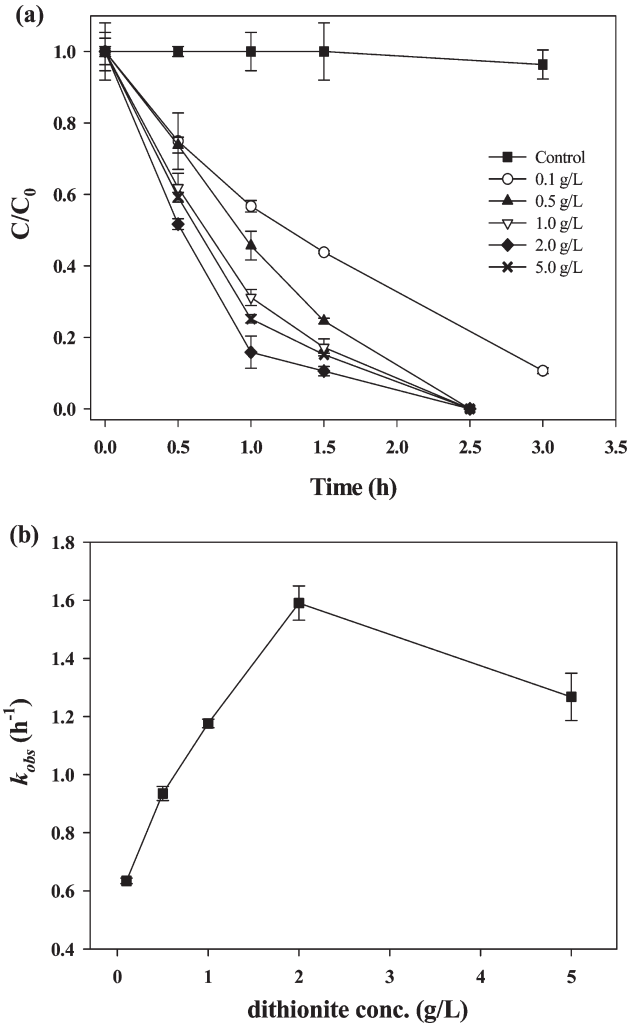

Figure 5. (a) Effect of dithionite loading on the removal rate of TCE by Fe/FeS ($[TCE]_0$ = 0.11 mM; [Fe/FeS] = 2 g/L). (b) Correlation between dithionite concentration and reaction rate constant.

constants (k_{obs}) increased linearly with increasing dithionite concentrations up to 2.0 g/L and, then, decreased when dithionite loading exceeded 2.0 g/L. The order of Fe/FeS 4 > Fe/FeS 5 > Fe/FeS 3 > Fe/FeS 2 > Fe/FeS 1 for k_{obs} and surface area-normalized rate constant (k_{sa}) were obtained (Table 2), and the sequence is in good agreement with the surface area results. However, we found little difference in the order of AFM/EFM R_{rms} values and above rate constants. The possible explanation for this fact is that more FeS is formed with increasing levels of dithionite, which can block the active sites on the surface thereby inhibiting the dissolution of iron core. Indeed, by increasing dithionite concentration from 2.0 to 5.0 g/L, the E_h value increased from −592.9 to −480.2 mV. Similar phenomenon has been also observed in iron-based bimetallic systems.[39,40] For example, inadequate and excessive coating of Ni may lead to formation of Fe-rich area or Ni-rich area, which lowers the catalytic activity. Therefore, the highest reactivity of Fe/FeS 4 can be attributed to the optimal FeS arrangement on the Fe surface.

The TCE reduction capability of Fe/FeS 4 was compared with RNIP, Fe(B), and FeS (Figure 6). Fe/FeS exhibited a high reactivity toward TCE removal, and complete reduction was

Table 2. Rate Constants for TCE Reduction by Fe/FeS and Fe(B)

materials	k_{obs} (1/h)	k_{sa} (L/m^2·h)
Fe/FeS 1	0.634 (±0.010)	1.23 (±0.039) × 10^{-2}
Fe/FeS 2	0.935 (±0.024)	1.44 (±0.028) × 10^{-2}
Fe/FeS 3	1.06 (±0.151)	1.61 (±0.237) × 10^{-2}
Fe/FeS 4	1.59 (±0.059)	1.83 (±0.060) × 10^{-2}
Fe/FeS 5	1.30 (±0.039)	1.69 (±0.039) × 10^{-2}
Fe(B)	7.45 (±0.070) × 10^{-2}	1.43 (±0.014) × 10^{-3}

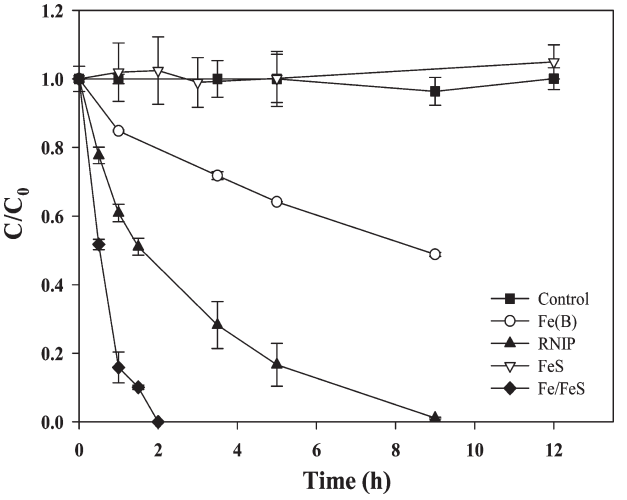

Figure 6. Removal of TCE by Fe(B), RNIP, FeS, and Fe/FeS ($[TCE]_0$ = 0.11 mM; [reductant] = 2 g/L).

achieved within less than 2 h. Small amounts of *cis*-DCE as an intermediate were detected during the reaction. Abiotic transformation of TCE by Fe or FeS occurs via at least two routes:[20,41,42] sequential hydrogenolysis (TCE → *cis*-DCE → vinyl chloride → ethylene) and β-elimination (TCE → chloroacetylene → acetylene). Previous studies have proposed that TCE degradation products may form by more than one pathway, and the branching ratio between competing reactions can be affected by experimental conditions, such as mixing efficiency and temperature.[41−43] Further works are in progress to determine the relative contribution of hydrogenolysis and reductive elimination on Fe/FeS through the analysis of product distribution. Almost 95% and 50% of TCE were reduced by RNIP and Fe(B) after 9 h of reaction. However, there was no measurable change in the amount of TCE in the presence of FeS for 12 h. The observed k_{sa} for Fe/FeS 4 was 1.83 × 10^{-2} L/m^2·h, which was approximately 12 and 2.5 times higher than those for Fe(B) (1.43 × 10^{-3} L/m^2·h) and RNIP (7.34 × 10^{-3} L/m^2·h), respectively. In addition, the rate constant of the synthesized Fe/FeS was much higher than the literature values for FeS (~2 × 10^{-3} L/m^2·h),[42] microscale (~10^{-4}−10^{-3} L/m^2·h)[44] and nanoscale Fe (1−2 × 10^{-3} L/m^2·h).[45,46] The results indicate that the Fe/FeS nanoparticles can be suitable and effective material for the removal of pollutants from contaminated water.

4. CONCLUSIONS

Herein, a novel and facile route for the synthesis of Fe/FeS nanoparticles has been developed, which exhibits the combined

advantages of both Fe and FeS materials. Characterization results clearly indicated that the inherent properties of pure Fe nanoparticles, such as electrical conductivity, magnetic susceptibility, and specific surface area, were greatly affected by the presence of FeS. The optimal arrangement between Fe and FeS phases was responsible for a strong reactivity of the nanoparticles toward contaminants. The Fe/FeS was significantly more efficient than previously reported techniques for the removal of TCE. The Fe/FeS nanoparticles have potential applications as reductants and sorbents in contaminated water treatments.

AUTHOR INFORMATION

Corresponding Author

*Phone: +82-54-279-2281. Fax: +82-54-279-8299. E-mail: yschang@postech.ac.kr.

ACKNOWLEDGMENT

This research was supported by Korea Ministry of Environment, "The GAIA project" and "The BK21 project".

REFERENCES

(1) Ajayan, P. M.; Schadler, L. S.; Braun, P. V. *Nanocomposite Science and Technology*; Wiley-VCH: Weinheim, 2004.
(2) Zeng, H.; Sun, S. *Adv. Funct. Mater.* **2008**, *18*, 391.
(3) Safarik, I.; Safarikova, M. *Solid State Phenom.* **2009**, *151*, 88.
(4) Dong, J.; Xu, Z.; Kuznicki, S. M. *Adv. Funct. Mater.* **2009**, *19*, 1268.
(5) Deng, C.; Yan, X.; Chen, H.; Lu, X. *J. Phys. Chem. C* **2009**, *113*, 21068.
(6) Guan, J. G.; Wang, W.; Gong, R. Z.; Yuan, R. Z.; Gan, L. H.; Tam, K. C. *Langmuir* **2002**, *18*, 4198.
(7) Wang, Q.; Wu, A.; Yu, L.; Liu, Z.; Xu, W.; Yang, H. *J. Phys. Chem. C* **2009**, *113*, 19875.
(8) Heidarpour, A.; Karimzadeh, F.; Enayati, M. H. *J. Alloy. Compd.* **2009**, *477*, 692.
(9) Fang, C. -L.; Qian, K.; Zhu, J.; Wang, S.; Lv, X.; Yu, S. -H. *Nanotechnology* **2008**, *19*, 125601.
(10) Marita, Y.; Yaacob, I. I. *Adv. Mater. Res.* **2010**, *97−101*, 1360.
(11) Wellons, M. S.; Morris, W. H., III; Gai, Z.; Shen, J.; Bentley, J.; Wittig, J. E.; Lukehart, C. M. *Chem. Mater.* **2007**, *19*, 2483.
(12) Zhang, X.; Wang, B.; Xu, X. *Appl. Surf. Sci.* **2010**, *256*, 4109.
(13) Bonetti, E.; Del Bianco, L.; Signoretti, S.; Tiberto, P. *J. Appl. Phys.* **2001**, *89*, 1806.
(14) Rickard, D.; Luther, G. W., III *Chem. Rev.* **2007**, *107*, 514.
(15) Min, Y.; Chen, Y.; Zhao, Y. *Solid State Sci.* **2009**, *11*, 451.
(16) Watson, J. H. P.; Cressey, B. A.; Roberts, A. P.; Ellwood, D. C.; Charnock, J. M.; Soper, A. K. *J. Magn. Magn. Mater.* **2000**, *214*, 13.
(17) Haaijer, S. C. M.; Lamers, L. P. M.; Smolders, A. J. P.; Jetten, M. S. M.; Op de Camp, H. J. M. *Geomicrobiol. J.* **2007**, *24*, 391.
(18) Lipszynska-Kochany, E.; Harms, S.; Milburn, R.; Sparh, G.; Nadarajah, N. *Chemosphere* **1994**, *29*, 1477.
(19) Butler, E. C.; Hayes, K. F. *Environ. Sci. Technol.* **1998**, *32*, 1276.
(20) Butler, E. C.; Hayes, K. F. *Environ. Sci. Technol.* **2001**, *35*, 3884.
(21) He, Y. T.; Wilson, J. T.; Wilkin, R. T. *Environ. Sci. Technol.* **2008**, *42*, 6690.
(22) Hua, B.; Deng, B. *Environ. Sci. Technol.* **2008**, *42*, 8703.
(23) Sun, Q.; Feitz, A. J.; Guan, J.; Waite, T. D. *Nano* **2008**, *3*, 341.
(24) Boparai, H. H.; Shea, P. J.; Comfort, S. D.; Snow, D. D. *Environ. Sci. Technol.* **2006**, *40*, 3043.
(25) Holman, D. A.; Bennett, D. W. *J. Phys. Chem.* **1994**, *98*, 13300.
(26) Hassan, S. M. *Chemosphere* **2000**, *40*, 1357.
(27) De Carvalho, L. M.; Schwedt, G. *Anal. Chim. Acta* **2001**, *436*, 293.
(28) Kim, J.-H.; Tratnyek, P. G.; Chang, Y.-S. *Environ. Sci. Technol.* **2008**, *42*, 4106.
(29) Jeong, H. Y.; Lee, J. H.; Hayes, K. F. *Geochim. Cosmochim. Acta* **2008**, *72*, 493.
(30) Mullet, M.; Boursiquot, S.; Abdelmoula, M.; Genin, J. M.; Ehrhardt, J. J. *Geochim. Cosmochim. Acta* **2002**, *66*, 829.
(31) Boursiquot, S.; Mullet, M.; Abdelmoula, M.; Genin, J. M.; Ehrhardt, J. J. *Phys. Chem. Minerals* **2001**, *28*, 600.
(32) Henke, L.; Nagy, N.; Krull, U. J. *Biosens. Bioelectro.* **2002**, *17*, 547.
(33) Gotpagar, J.; Lyuksyutov, S.; Cohn, R.; Grulke, E.; Bhattacharyya, D. *Langmuir* **1999**, *15*, 8412.
(34) Luo, S.; Yang, S.; Wang, X.; Sun, C. *Chemosphere* **2010**, *79*, 672.
(35) Vaughan, D. J.; Ridout, M. S. *J. Inorg. Nucl. Chem.* **1971**, *33*, 741.
(36) Liu, Y.; Choi, H.; Dionysiou., D.; Lowry, G. V. *Chem. Mater.* **2005**, *17*, 5315.
(37) Ponder, S. M.; Darab, J. G.; Mallouk, T. E. *Environ. Sci. Technol.* **2000**, *34*, 2564.
(38) Cullity, B. D.; Graham, C. D. *Introduction to Magnetic Materials*, 2nd edition; Wiley-IEEE Press: NJ, 2009.
(39) Xu, J.; Bhattacharya, D. *Environ. Prog.* **2005**, *24*, 358.
(40) Parshetti, G. K.; Doong, R. A. *Water Res.* **2009**, *43*, 3086.
(41) Arnold, W. A.; Roberts, A. L. *Environ. Sci. Technol.* **2000**, *34*, 1794.
(42) Butler, E. C.; Hayes, K. F. *Environ. Sci. Technol.* **1999**, *33*, 2021.
(43) Li, T.; Farrell, J. *Environ. Sci. Technol.* **2001**, *35*, 3560.
(44) Johnson, T. L.; Scherer, M. M.; Tratnyek, P. G. *Environ. Sci. Technol.* **1996**, *30*, 2634.
(45) Schrick, S. M.; Darab, J. G.; Mallouk, T. E. *Chem. Mater.* **2002**, *14*, 5140.
(46) Wang, C.-B.; Zhang, W.-X. *Environ. Sci. Technol.* **1997**, *31*, 2154.